Soft Matter

RSC Publishing

PAPER

View Article Online
View Journal | View Issue

A tension-based model of flat and corrugated simple epithelia

Cite this: *Soft Matter*, 2013, **9**, 8368

M. Krajnc,†[ab] N. Štorgel,†[ab] A. Hočevar Brezavšček[cb] and P. Ziherl*[ab]

We theoretically study the shape of single-cell-thick epithelium consisting of incompressible fluid cells. The cells carry a surface energy associated with cortex and interfacial tension as well as cell–cell adhesion such that the basal, the lateral, and the apical cell faces are each characterized by a specific effective surface tension. In our reduced-dimensionality version of the model, the epithelium consists of a linear chain of quadrilateral cells. We explore the 1D periodic minimal-energy configurations of the tissue, finding that they include both flat and corrugated states. As the differential apical-basal tension is increased, the epithelium undergoes a transition from the thin flat state to the expanded corrugated state which is then compactified and transformed into the collapsed corrugated state and eventually replaced by the thick flat state. Apart from the restriction to the globally uncurved space, the corrugated states are shaped by apical constriction and cell impenetrability. We also analyze the elastic properties of these states, focusing on the stretching modulus and the torque exerted on the substrate.

Received 7th June 2013
Accepted 10th July 2013

DOI: 10.1039/c3sm51588e

www.rsc.org/softmatter

Introduction

Mechanics of elastic sheets is packed with fascinating examples of shape formation. A clamped stretched sheet will develop regular wrinkles[1] and the edge of a torn sheet is decorated by a hierarchy of waveforms best referred to as the buckling cascade.[2] In the latter case, the delicate structures seen along the edge are due to the differential deformation and the resulting internal stresses which are partly relieved by buckling. In sheets and patches with a pre-programmed pattern of area shrinking or expansion, a suitable external stimulus such as heat or hydration activates the desired 3D shape which can be fairly elaborate.[3,4]

In living matter, internal stresses leading to nontrivial morphologies of sheet-like structures can be caused by cell growth and division.[5] Yet even in the most plain cellular thin sheet—the simple epithelium—they can also arise from intracell forces, notably from the acto-myosin contractile network.[6–8] As hypothesized in the seminal mechanical theory of morphogenesis,[9] these forces can be probed with advanced force-microscopy techniques[10,11] and their relevance is witnessed, *e.g.*, by the behavior of *Xenopus laevis* embryonic epithelial explants which readily curve to form a spherule or curl into a spiral roll.[12]

Here we theoretically analyze a mechanical model of a single-cell-thick epithelium which is characterized primarily by internal stresses and much less by the interaction with the supporting tissues. Our aim is to check whether this model can qualitatively reproduce the typical epithelial morphologies such as various invaginations and infoldings seen in embryonic development[9,13] and the nonuniform topography of villi, crypts or herringbone ripples in the intestinal epithelia. By doing so we wish to establish which of these structures are driven or controlled mainly by intra-epithelial forces and which rely on the surrounding tissues as well as on cell growth and division and other active processes.

Our model assumes that the cell interior is fluid and that cell shape is determined by tensions of the three types of cell sides: the basal side attached to the basement membrane, the lateral side where cells adhere to each other, and the apical side which faces the lumen.[14] This framework has been used to describe the transverse cross-section of the *Drosophila melanogaster* embryonic epithelium during the formation of the lengthwise invagination called the ventral furrow.[15] In this theory, one of the key elements driving the invagination is the localized constriction of a small segment of cells caused by large enough differences between the three tensions. But the shape of the *Drosophila* embryo is determined jointly by the forces within the epithelium itself as well as by the constraints due to the incompressible yolk core and the semi-hard vitelline membrane around the epithelium. As a result, the importance of constrictions is somewhat obscured and one cannot readily tell how far-reaching is the intra-tissue mechanics alone.

In this paper, we concentrate on the role of cell constrictions in epithelial morphogenesis. We study a model infinite epithelium supported by a substrate which ensures that the tissue remains globally uncurved but does not directly affect its

[a]*Faculty of Mathematics and Physics, University of Ljubljana, Jadranska 19, SI-1000 Ljubljana, Slovenia. E-mail: primoz.ziherl@ijs.si*

[b]*Jožef Stefan Institute, Jamova 39, SI-1000 Ljubljana, Slovenia*

[c]*Center for Studies in Physics and Biology, Rockefeller University, 1230 York Avenue, New York, NY 10065-6399, USA*

† These authors contributed equally to this work.

shape in any other way. We choose to analyze the behavior of the reduced-dimensionality variant of the problem where epithelial cells are represented by trapezoidal planar figures arranged on a 1D chain rather than by prismatic solid bodies forming a 2D sheet. First we show that depending on the relative apical and basal tensions, the energy-minimizing shape of the epithelium can be either flat or corrugated, which implies that the internal stresses within tissues alone can generate nontrivial ground states. We also analyze the mechanical properties of the equilibrium states, finding that the flat shapes are generally stiffer than the corrugated shapes. Finally we discuss some implications of these results for real epithelia.

The model

Our mechanical model of the single-cell-thick epithelium (Fig. 1a) is based on the assumption that the shape of the tissue corresponds to the minimal-energy state, tacitly neglecting any dynamic effects related to cell viscosity which is consistent with slow relaxation towards equilibrium. We furthermore assume that the cells are filled with an incompressible Newtonian fluid and that their energy resides in the cell membrane only, leaving out the elasticity of cytoskeleton. This approximation is not as crude as it may seem because as elaborated below in the discussion of tissue stretching, our model cells still have a finite shear modulus as if they were characterized by bulk elasticity.

The advantage of exploring a stripped-down rather than a faithful representation of the tissue is in emphasizing the workings of the different mechanisms that may give rise to nontrivial tissue morphologies, and the main cause of tissue deformation studied here is the membrane-based intra-cell stress within an equilibrium, minimal-energy theory. The microscopic origin of membrane energy is threefold: (i) cortex tension acting across all of the membrane, (ii) adhesion between neighboring cells which is characteristic of the lateral sides, and (iii) differential apical-basal tension which distinguishes cell–lumen contact from cell–basement membrane contact (Fig. 1b). The energies associated with these three terms are all proportional to area of the cell side in question.

The 2D version of the model discussed here may be regarded as the cross-section of the epithelium that is unmodulated in the transverse direction perpendicular to the cross-section. The quadrilateral model cell outline represents the longitudinal cutaway of an epithelial prismatic cell. Furthermore, if we assume that the length of tissue and the size of cells in the transverse direction are fixed then the fixed-cell-volume constraint implies that the area of the outline of our model cells is constant ($A = \text{const.}$).

The energy of a single cell reads

$$W = \sigma(L_a + L_b + L_l) + \eta(L_b - L_a) - \frac{\gamma}{2}L_l, \quad (1)$$

where σ is the cortex tension, η describes the asymmetry of tensions of apical and basal sides, and γ is the adhesion strength; L_a, L_b, and L_l are the lengths of the apical, basal, and lateral sides.[14] Alternatively, the single-cell energy can be expressed in terms of the effective tensions of apical, basal, and lateral sides so that

$$W = \Gamma_a L_a + \Gamma_b L_b + \frac{1}{2}\Gamma_l L_l. \quad (2)$$

To ensure stability, Γ_a, Γ_b, and Γ_l must be positive.

The two representations [eqn (1) and (2)] are equivalent and each has its advantages. The (σ, η, γ) parameterization is based on quantities of clear microscopic interpretation but the effective tensions $\Gamma_a = \sigma - \eta$, $\Gamma_b = \sigma + \eta$, and $\Gamma_l = 2\sigma - \gamma$ are more directly measurable.[10] This is why we here stick to the effective tensions although we will often interpret the results using reduced variants of tissue lateral tension $\Gamma_a + \Gamma_b = 2\sigma$ and differential tension $\Gamma_a - \Gamma_b = 2\eta$.

It is convenient to express all lengths in terms of $\sqrt{A}$ so that $l_i = L_i/\sqrt{A}$ are the reduced edge lengths and the dimensionless energy per cell reads

$$w = \frac{W}{\Gamma_l\sqrt{A}} = \alpha l_a + \beta l_b + \frac{1}{2}l_l, \quad (3)$$

where

$$\alpha = \frac{\Gamma_a}{\Gamma_l} \text{ and } \beta = \frac{\Gamma_b}{\Gamma_l} \quad (4)$$

are the reduced apical and basal tension, respectively; $\alpha + \beta$ is the reduced tissue lateral tension and $\alpha - \beta$ is the reduced differential tension. In the following, exclusively the reduced tensions are used and for the sake of brevity the designation "reduced" is omitted. Given that there is no formal distinction between the apical and the basal sides of the model epithelium and the energy is unchanged if α and β are swapped, the phase diagram of the equilibrium shapes obtained by minimizing the epithelium energy [eqn (3)] at a given α and β is symmetric about the diagonal $\alpha = \beta$. Here we describe the epithelium for $\alpha \geq \beta > 0$, typically varying α at fixed β.

As the main driving force for virtually all structures discussed here is the cell constriction driven by the difference between α and β, it is instructive to first examine the equilibrium shape of isolated cells. We assume that the cell edges are straight and that cells are isosceles trapezoids; these shapes include the rectangle and the isosceles triangle as the limiting cases. By minimizing eqn (3) at fixed area we find that the energy of the trapezoidal cell reads

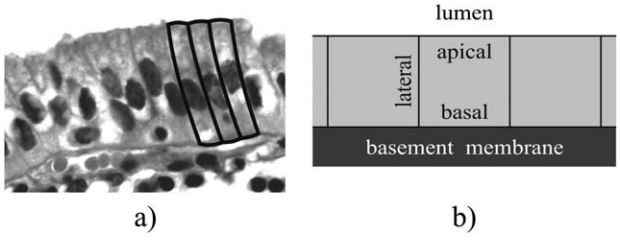

Fig. 1 Simple columnar epithelium of the gallbladder mucous membrane (panel a; image courtesy of D. Petrovič) with highlighted contours of three cells. Schematic of the model epithelium (panel b): cells' apical sides are adjacent to lumen, their basal sides rest upon the basement membrane, and neighboring cells adhere to each other by their lateral sides.

$$w_{\mathrm{trap}} = 2\sqrt{\alpha+\beta}\left[1-(\alpha-\beta)^2\right]^{1/4}, \quad (5)$$

their height being given by $l_{\mathrm{trap}} = \sqrt{\alpha+\beta}/[1-(\alpha-\beta)^2]^{1/4}$. For $\alpha = \beta$, this result reduces to $w_{\mathrm{rect}} = 2\sqrt{\alpha+\beta}$ corresponding to rectangular shapes of height $l_{\mathrm{rect}} = \sqrt{\alpha+\beta}$. Note that the cells are square for $\alpha = \beta = 1/2$ (*i.e.*, for $\alpha + \beta = 1$ and $\alpha - \beta = 0$).

As the apical tension α is increased at fixed basal tension β, the apical edge gradually shrinks until it vanishes at

$$\alpha_{\mathrm{t}} = \frac{1}{2}\left(\beta + \sqrt{2+\beta^2}\right) \quad (6)$$

and the trapezoid assumes the shape of a triangle which no longer depends on the apical tension. The triangle energy reads

$$w_{\mathrm{tria}} = \frac{2\beta + \sqrt{2\left(1+\beta^2+\beta\sqrt{2+\beta^2}\right)}}{\left(1+2\beta^2+2\beta\sqrt{2+\beta^2}\right)^{1/4}} \quad (7)$$

and the triangle height is $l_{\mathrm{tria}} = \left(1+2\beta^2+2\beta\sqrt{2+\beta^2}\right)^{1/4}$.

The stability of the trapezoidal shapes is restricted to a stripe centered at zero differential tension $\alpha - \beta$ (shaded region in Fig. 2). Fig. 2 also shows four sequences of shapes at fixed basal tension which illustrate that the cell intrinsic curvature (defined as the inverse distance between the trapezoid median and the point of intersection of lines passing through the lateral sides) increases with α until the cells become triangular. In the triangular regime, the shape of cells is independent of apical tension α and their curvature is more pronounced at small basal tensions β.

The intrinsic curvature of isolated cells implies that the energy-minimizing, stress-free epithelium must be ring-like and contain a finite number of cells, qualitatively similar to the spherules formed by explants from the *Xenopus laevis* embryo.[12] However, if the integrity of the infinite epithelium is not disrupted and if the cells remain connected not all of them can undergo apical constriction at a large enough differential tension $\alpha - \beta$. In this case the minimal-energy configurations of an infinite epithelium are molded both by cells' intrinsic curvature and by the hard-core repulsion between them.

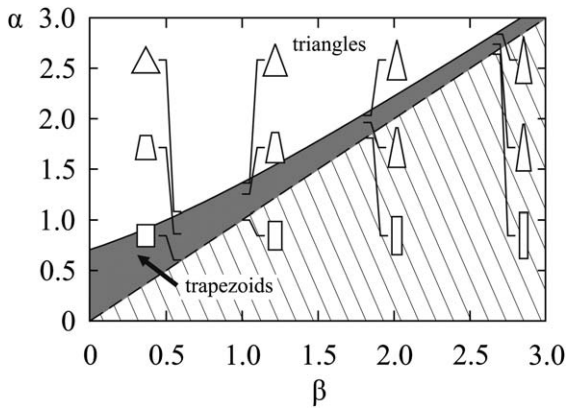

Fig. 2 Equilibrium shapes of isolated cells include rectangles (which lie on the diagonal $\alpha = \beta$ indicated by the dashed line), trapezoids (shaded region), and triangles at $\alpha > \alpha_{\mathrm{t}}$ [white region; solid line shows $\alpha_{\mathrm{t}}(\beta)$]. Insets show a few typical shapes at basal tensions $\beta = 0.6$, 1.0, 1.8 and 2.6. Large basal tensions ($\beta = 1.8$ and 2.6) correspond to tall cells whereas for $\beta \approx 0.5$ the cells are isometric. The hatched area indicates the $\beta < \alpha$ part of the phase diagram which is symmetric about the diagonal $\alpha = \beta$.

Ground states

After analyzing isolated cells, we turn to the shape of model epithelium represented by an infinite 1D chain of cells resting on a substrate which enforces that the tissue is globally uncurved. Unlike earlier theories of epithelial morphologies which rely on the elastic response of the substrate,[16,17] our model is more akin to an epithelium floating on the surface of a liquid in the sense that we exclude the coupling between the deformation of the substrate and the tissue shape. We study the ground states by numerically minimizing the energy of the epithelium [eqn (3)] subject to periodic boundary conditions; this is implemented within the Surface Evolver package.[18] As neither the wavelength λ of the waveform nor the number of cells N in it can be estimated in advance, the global minimum of the energy at a given (α, β) is sought by varying both N and λ. For each structure we compute the average energy per cell and by comparing them we find that for both very similar and very dissimilar apical and basal tensions the equilibrium state is a flat epithelium whereas between these two regimes the stable states are non-trivial (Fig. 3).

Fig. 3a shows a sequence of equilibrium shapes at fixed basal tension $\beta = 0.6$. We note that the flat epithelium consisting of rectangular cells is stable until the reduced apical tension reaches a fairly large value. At $\alpha \approx 1.9$, the flat epithelium undergoes a transition to the expanded corrugated state (Fig. 3a, $\alpha = 2.2$) characterized by a contiguous segment of triangular cells exhibiting apical constriction. These cells form a hairpin bend at the tip of a protrusion whereas the remaining cells in the waveform are trapezoidal and arranged in an open arch. The corrugated epithelium can be viewed as a combination of a favorable and an unfavorable bend. The constricted hairpin cells indeed lower the energy relative to the flat epithelium whereas energy of the opposite-curvature trapezoidal cells of the arch needed to complete the waveform is larger than that of flat cells. A closer inspection shows that the triangular constricted cells are taller and less curved than the isolated cells at the respective α and β, and thus their energy is not as low as in isolated cells. On the other hand, the number of tall constricted cells that can fit in the hairpin turn is larger than the number of the more curved minimal-energy isolated cells, and apparently the combination of these two effects is favorable at the level of the whole waveform.

As α is increased further, the expanded corrugated state gradually collapses (Fig. 3a). The total number of cells in the waveform decreases and so does the wavelength. The collapse primarily affects the unfavorable bend, which becomes smaller and narrower and contains fewer cells than in the expanded state. Some cells of the unfavorable bend are forced into a pronounced trapezoidal basally constricted shape. Simultaneously, the number of cells in the favorable bend is slightly increased and they become somewhat taller than in the

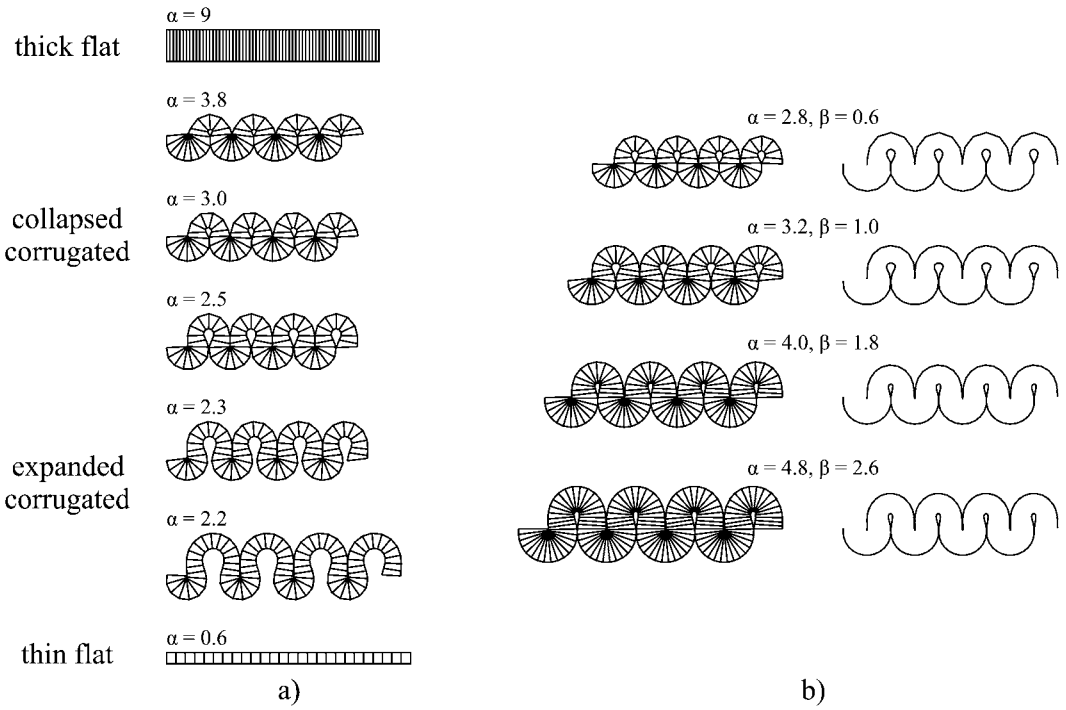

Fig. 3 Representative ground states at fixed basal tension $\beta = 0.6$ (panel a): thin flat ($\alpha = 0.6$), expanded corrugated ($\alpha = 2.2$ and 2.3), collapsed corrugated ($\alpha = 2.5$, 3, and 3.8), and thick flat epithelium ($\alpha = 9$). Panel b shows four examples of corrugated epithelia of dissimilar (α, β) but identical $\alpha - \beta$ and virtually indistinguishable shape. The close similarity of their shapes is emphasized by the contours of the apical and the basal surface scaled to same size (rightmost column).

expanded corrugated state. The touching sides of the non-neighboring cells in the collapsed corrugated state are assumed to retain their distinct functionality different from that of the lateral sides and do not adhere to each other. Thus the interaction of the non-neighboring cells is restricted to hard-core repulsion between them, which is clearly very important for the global shape of the epithelium.

The collapsed corrugated state is robust in the sense that its morphology is virtually the same across a broad range of apical tensions. Yet beyond some large α, this state is replaced by the thick flat epithelium which then persists at arbitrarily large apical tensions. The distinction between the thin and the thick flat epithelia is merely quantitative: At fixed β, the latter consists of taller cells than the former.

The model epithelia seen at other values of the reduced basal tension β are similar to those shown in Fig. 3a. This is illustrated in Fig. 3b where we compare the corrugated ground states at four different (α, β) but identical differential tension $\alpha - \beta$. The large features of their shapes—the contour, the ratio of height and wavelength, *etc.*—are quantitatively almost identical, which is clearly demonstrated by the apical and basal surfaces of the four waveforms scaled to same size (right column of Fig. 3b). As α and β are increased the cells become taller and taller, which makes the epithelium thicker and its wavelength longer. Yet the shape of the tissue converges.

The most interesting structural feature of the corrugated state is the wavelength λ_{eq}. Its dependence on the apical tension α is shown in Fig. 4 which reveals two clearly separated regimes. At α immediately beyond the transition between the flat and the expanded corrugated states, λ_{eq} rapidly decreases with α, the decrease indicating the collapse of the expanded state. This regime is followed by a slight increase of the wavelength with the apical tension. At small basal tensions ($\beta = 0.6$ and 1.0 in Fig. 4) the difference between the saturated value of λ at large α and the minimum is negligible whereas at large β (1.8 and 2.6 in Fig. 4) it reaches about 10%. The equilibrium number of cells in a waveform shown in the inset to Fig. 4 varies in a similar way except that it decreases monotonically and considerably more gradually than the wavelength.

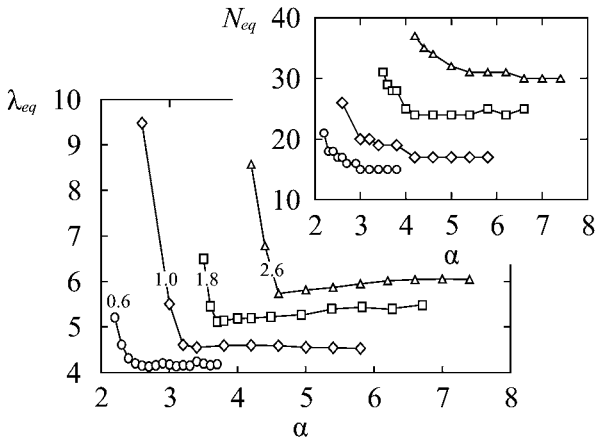

Fig. 4 Equilibrium wavelength of the corrugated waveforms for basal tension $\beta = 0.6$, 1.0, 1.8 and 2.6 (circles, diamonds, squares, and triangles, respectively). Inset: equilibrium number of cells in the corrugated waveforms for the four values of β.

Our numerical insight allows us to outline the phase diagram of the epithelium (Fig. 5). We scanned the phase diagram at four values of basal tension corresponding to weak ($\beta = 0.6$), intermediate ($\beta = 1$), and strong ($\beta = 1.8$ and 2.6) cell-basement membrane tension. At each β we computed a sequence of flat and corrugated shapes and we estimated the locations of the transitions between them.

By comparing the analytical energy of the flat state $w_{\mathrm{rect}} = 2\sqrt{\alpha+\beta}$ to the numerically evaluated energy of the corrugated state (somewhat extrapolated to locate the transition), we find that the boundary between the two types of epithelia increases with β, the increase being linear at $\beta > 1$. At small β, the transition deviates from the large-β linear trend which may suggest that the behavior of the epithelium in the "squamous" regime where the width of cells is much larger than their height departs from the results presented here. This uncharted and possibly special regime is indicated by the fade-out white region in Fig. 5.

The transition from the expanded to the collapsed corrugated state is a little harder to pin down exactly as the distinction between the two states is somewhat arbitrary. In Fig. 5, we chose to associate it with the shape where the arch is just closed [*e.g.*, shape ($\alpha = 2.5$, $\beta = 0.6$) in Fig. 3a]. Within the range of β studied here, these transitions appear to lie on a straight line.

Finally, the collapsed corrugated to thick flat transition was estimated by extrapolating the energy of the former to large α and comparing it to the energy of the flat state. At a large α, the shape of the collapsed corrugated waveform saturates and both the number of cells in the waveform and the proportions of each individual cell no longer depend on α. As a result, its energy is a linear function of the reduced apical tension α and for large enough α it exceeds the energy of a flat epithelium given by $w_{\mathrm{rect}} = 2\sqrt{\alpha+\beta}$. As the two energies typically intersect at a shallow angle, the location of the transition depends very much on the accuracy of the extrapolated energy of the corrugated state. This gives rise to a considerable error and the error bars in Fig. 5 were obtained by estimating the inaccuracy of the numerical derivative of the energy of the corrugated state $\partial w_{\mathrm{corr}}/\partial\alpha$.

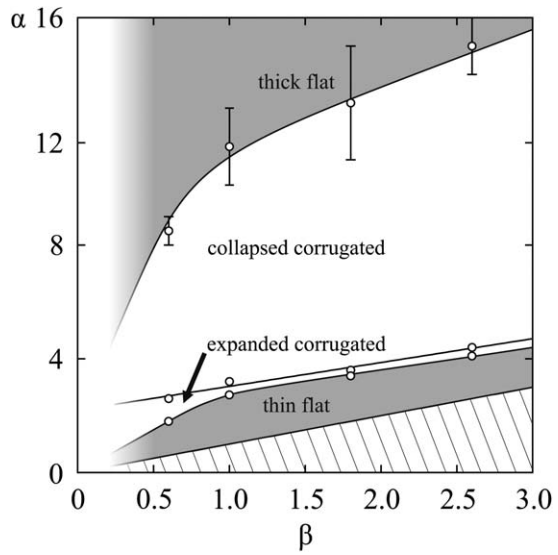

Fig. 5 Phase diagram of the model epithelium in the (β, α) plane. The lines connecting the numerically estimated transitions at $\beta = 0.6$,1,1.8, and 2.6 (open symbols) are guides to the eye. Unless indicated, the error bars are no larger than the symbols. The meaning of the hatched area is the same as in Fig. 3.

Based on the known morphological features of corrugated epithelia, we can construct an approximate theory of the transition from the thin flat to the expanded corrugated state. Our starting point is the assumption that to second order in cell curvature c, the energy of a cell in either the flat or corrugated state reads

$$w(c) = w_{\mathrm{tria}} + \frac{Yl_{\mathrm{m}}}{2}(c - c_0)^2, \tag{8}$$

where w_{tria} is the energy of the isolated triangular cells at a given β whereas Y, l_{m}, and c_0 are their bending modulus, width, and spontaneous curvature, respectively. A comparison of the $\alpha =$ 2.2, 2.3, and 2.5 waveforms shown in Fig. 3 suggests that the corrugated state consists of a fixed number N_{t} of triangular cells and of a variable number N_{u} of cells in the unfavorable bend. The curvature of the triangular cells (c') is of the same sign but somewhat smaller than c_0, and their energy reads $w_{\mathrm{tria}} + Yl_{\mathrm{m}}(c' - c_0)^2/2$. The unfavorable bend is semicircular, its curvature c being of opposite sign than c_0 and related to the perimeter of the bend by $c = -1/r = -\pi/N_{\mathrm{u}}l_{\mathrm{m}}$ where l_{m} is cell width. In terms of the fraction of cells in the unfavorable bend

$$x = \frac{N_{\mathrm{u}}}{N_{\mathrm{t}} + N_{\mathrm{u}}}, \tag{9}$$

the average energy per cell in the expanded corrugated waveform is approximately given by $w_{\mathrm{corr}}(x) = w_{\mathrm{tria}} + Yl_{\mathrm{m}}\{(1 - x)(c' - c_0)^2 + x[\pi(1 - x)/(N_{\mathrm{t}}l_{\mathrm{m}}x) + c_0]^2\}/2$. We now compare w_{corr} to the energy of cells in the flat state $w_{\mathrm{flat}} = w(c = 0) = w_{\mathrm{tria}} + Yl_{\mathrm{m}}{c_0}^2/2$. Their difference $\Delta w(x) = w_{\mathrm{corr}}(x) - w_{\mathrm{flat}}$ is given by

$$\Delta w(x) = \frac{Y{c_0}^2 l_{\mathrm{m}}}{2}\left[(1-x)(\omega-1)^2 + x\left(\frac{1-x}{x}\xi + 1\right)^2 - 1\right]. \tag{10}$$

where $\omega = c'/c_0$ and $\xi = \pi/(N_{\mathrm{t}}l_{\mathrm{m}}c_0)$ are dimensionless parameters inversely proportional to the spontaneous curvature of the cells. It is not hard to see that for large ω and ξ, $\Delta w(x)$ is minimized by $x = 1$ where $\Delta w = 0$ which corresponds to the flat state. On the other hand, for small enough ω and ξ the energy difference develops a minimum at $x < 1$ where $\Delta w < 0$. This minimum represents the corrugated state. Thus the flat-corrugated transition can be induced by increasing the cell spontaneous curvature, thereby decreasing both ω and ξ. This indeed happens as the apical tension is increased at fixed basal tension.

The most striking feature of the phase diagram is the reentrant flat–corrugated–flat transition which can be qualitatively rationalized as follows. At vanishing differential tension $\alpha - \beta$ where isolated cells are rectangular the flat epithelium is the minimal-energy configuration even in the absence of periodic boundary conditions. As argued above, the corrugated state is favored at intermediate differential tension because it allows some of the cells in the waveform to adopt the apically

constricted triangular shape and the energy cost of the unfavorable bend is not too big. But as the differential tension is increased, the corrugated epithelium eventually converges to a limiting shape which is unable to adapt to a further increase of the differential tension. On the other hand, cells in the flat epithelium do become taller and taller as the apical tension is increased, which is why their energy grows more gradually compared to the corrugated state. As a result, the thick flat epithelium is stable at large differential tensions.

The broad features of the phase diagram (Fig. 5) can be further refined. In particular, it is possible that there exist wavy derivatives of the flat states. Characterized by a sinusoidal contour, trapezoidal unconstricted cells, and long wavelength, such states could conceivably be stable at small differential tensions but may prove numerically demanding due to the large number of cells in the waveform. Instead, a continuum version of the discrete, cell-based model could well be more suitable for the description of the smoothly undulating, long-wavelength configurations.

Another limit of the model not discussed here is the behavior of the epithelium at very small basal tension $\beta \ll 1$. In this regime cells should tend toward flattened shapes reminiscent of the squamous epithelium and the quantitative effect of the differential tension should be more pronounced than at $\beta \approx 1$. By comparing the shapes in Fig. 3b, we expect that the small-β corrugated waveform should contain very few cells. In this case the cell–cell repulsion will be even more important for the stabilization of the waveform, possibly leading to epithelial morphologies which may depart from those reported in Fig. 3. This regime is computationally more demanding and will be addressed in future work.

Epithelial elasticity

Given the structural disparity between the flat and corrugated states, it is natural to expect that their mechanical properties should be different. One aspect of epithelial elasticity which is of obvious biological relevance is the response of epithelium to stretching or compression. Secondly, as the corrugated states are driven by differential tension leading to apical constriction it can be expected that they should tend toward a curved configuration and that a certain torque is needed to maintain the overall planarity of the epithelium. Below we address these two issues in detail.

Stretching modulus

Upon dilation or compression, the energy of the epithelial waveform is increased. The strain is given by $\delta\lambda/\lambda_{eq}$ where λ_{eq} and $\delta\lambda$ are the equilibrium wavelength and its variation, respectively. To the lowest order the variation of energy per unit length of the waveform reads

$$\frac{N_{eq}\delta w}{\lambda_{eq}} = \frac{\kappa}{2}\left(\frac{\delta\lambda}{\lambda_{eq}}\right)^2, \tag{11}$$

where N_{eq} is the equilibrium number of cells in the waveform and δw is the variation of the average energy per cell. Eqn (11) serves as the definition of the reduced stretching modulus κ. For the flat epithelium κ can be computed analytically: in this case $N_{eq} = 1$ and λ_{eq} is equal to the equilibrium cell width $l_{eq} = 1/\sqrt{\alpha+\beta}$, giving

$$\kappa_f = 2(\alpha + \beta). \tag{12}$$

The stretching modulus of the flat state is thus proportional to the tissue lateral tension $\alpha + \beta$, which is plausible and expected.[14] We note in passing that in the case of flat epithelium, stretching consists of uniaxial pure-shear deformation of individual cells and so these results can be recast to express the effective Young modulus E of a cell. In non-reduced units, the deformation energy per cell $\delta W = (1/2)\int E u_{zz}^2 dA$, where the in-plane strain $u_{zz} = \delta\lambda/\lambda_{eq}$. We find that E is given by $2\sqrt{(\Gamma_a+\Gamma_b)\Gamma_l/A} = 2\sqrt{\alpha+\beta}\,\Gamma_l/\sqrt{A}$. The finite value of E means that our model cells possess shear rigidity, and the dependence of the modulus on cell area $E \propto 1/\sqrt{A}$ is characteristic of the tension-based cell energy used here.

The modulus of the corrugated epithelium is obtained from the numerically computed dependence of the energy on the wavelength at a fixed number of cells N. By considering the family of curves at different N, we identify the minimal-energy states within a range of λ_{eq} around the optimal wavelength at a given α and β. These states are represented by the envelope of the fixed-N curves and κ of the corrugated epithelium is computed from the second derivative of the envelope at $\lambda = \lambda_{eq}$.

Fig. 6 combines the analytical stretching modulus of the flat state [eqn (12)] and the numerical corrugated-state results for the $\beta = 0.6$ and the $\beta = 2.6$ sequences representing small and large basal tension, respectively. For $\beta = 0.6$, the difference between the moduli of the flat and the corrugated states is quite dramatic, the latter being much softer than the former. In particular, at the transition between the thin flat and the

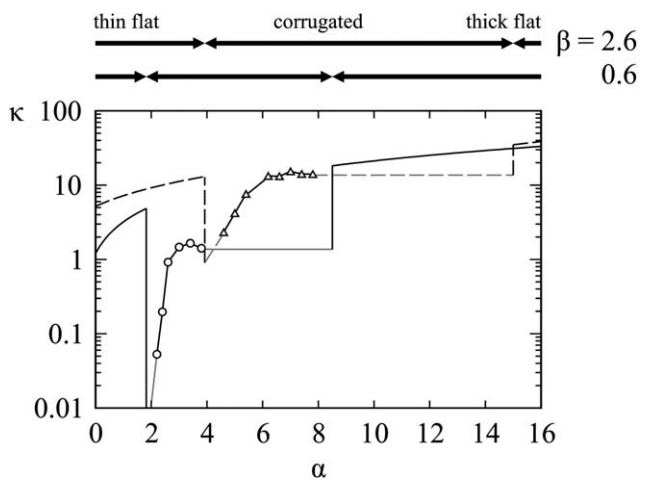

Fig. 6 Stretching modulus of the model epithelium for $\beta = 0.6$ (solid line) and $\beta = 2.6$ (dashed line). Solid line shows the analytical result for flat epithelium [eqn (12)] whereas the symbols represent the numerically computed modulus of the corrugated state. The lines connecting the symbols are guides to the eye and the gray lines are the extrapolated moduli of the corrugated state. The phase sequences are depicted by the arrows above the diagram.

expanded corrugated state κ drops by orders of magnitude. As the apical tension is increased further, the stretching modulus increases too until it levels off roughly at the transition between the expanded and the collapsed corrugated states. The horizontal central segment in Fig. 6 (solid gray line) represents the extrapolated modulus of the collapsed corrugated state. As α is increased, we expect that the stretching modulus should slowly grow too but based on the flat-state κ, the slope should be small. As it is hard to estimate the magnitude of this effect, we choose to indicate the extrapolated behavior by a constant value.

At $\beta = 2.6$ the dependence of the stretching modulus on the apical tension is qualitatively similar to that at $\beta = 0.6$ but the difference between the flat and the corrugated states is less pronounced. In the expanded corrugated state, κ is still smaller than in the thin flat state whereas in the collapsed corrugated state it reaches a considerable fraction of the flat-state modulus.

It is not difficult to visualize why the corrugated states are softer than the flat states. Upon dilation or compression, the contour of their waveform changes and so does the number of cells in the waveform. Thus a given strain is translated into a small shear deformation of any individual cell, leading to a soft stretching modulus. On the other hand, in the flat epithelium any macroscopic strain is directly transmitted to each cell, and this makes it more rigid. The quantitative difference of the moduli of the $\beta = 0.6$ and the $\beta = 2.6$ corrugated states can be attributed to the spread of cell shapes encoded, *e.g.*, by cell curvature. Fig. 3 shows that for $\beta = 0.6$, the variation of cell curvature along the corrugated waveform is considerably bigger than at $\beta = 2.6$. This suggests that upon compression or dilation the cells can adapt their shape considerably, thereby lowering the energy and the stretching modulus more efficiently.

Torque

Unless the differential tension vanishes, the equilibrium shape of isolated cells is trapezoidal or triangular and the cells are characterized by a finite spontaneous curvature. This means that as the epithelium is forced into a globally uncurved state by the periodic boundary conditions, it exerts a certain torque on the implicit support that imposes the boundary conditions. To ensure that the epithelium remains uncurved this torque must be counterbalanced by the support or else it will adopt a distorted configuration much like the *Xenopus laevis* embryonic ectodermal epithelium which rolls into a spiral shape after it has been peeled off the inner ectoderm.[12]

The torque exerted by the epithelium can be computed from the variation of the energy due to global curvature, *i.e.*, by comparing the energy of the uncurved state to that of the curved state (Fig. 7). Upon bending, the angle between a pair of equivalent lateral edges of the waveform is increased from 0 to some small $\delta\phi$ and the energy is changed by work done by the torque on either face given by $m\delta\phi$. For pure bending $\delta\phi$ is related to the reduced curvature of the epithelium δc by

$$\delta\phi = \lambda_{\mathrm{eq}}\delta c \tag{13}$$

so that the average reduced torque per cell is given by

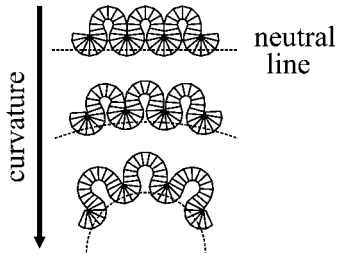

Fig. 7 Geometry of bent corrugated epithelia. Curvature increases from top to bottom, dashed arcs indicating the neutral lines.

$$m = \frac{N_{\mathrm{eq}}}{\lambda_{\mathrm{eq}}}\left.\frac{\delta w}{\delta c}\right|_{c=0}, \tag{14}$$

where w is the average energy per cell and N_{eq} is the equilibrium number of cells in the waveform.

The torque of the flat epithelium can be calculated analytically. Upon bending, the cell shape becomes slightly trapezoidal rather than rectangular and after a straightforward calculation we find that

$$m_{\mathrm{f}} = \frac{\sqrt{\alpha+\beta}(\alpha-\beta)}{2}. \tag{15}$$

As expected, the torque is proportional to the differential tension $\alpha - \beta$. The remainder of the numerator represents the height of rectangular cells $l_{\mathrm{l}} = \sqrt{\alpha+\beta}$, implying that the torque required to uncurve flat epithelia increases with tissue thickness.

In the corrugated epithelium, the torque is computed by considering a finite number Z of waveforms arranged on a circle. Given the known equilibrium number of cells per uncurved waveform N_{eq} at a given α and β, we construct a ring of ZN_{eq} cells and relax it to find the minimal-energy shape. The equilibrium shape of the ring is flower-like, its curvature being positive if the basal side faces the center of curvature and negative otherwise. To ensure that the deformation is pure bending, the radius of curvature is computed from the perimeter of the neutral circle equal to $Z\lambda_{\mathrm{eq}}$ so that the reduced curvature reads

$$c = \frac{1}{r} = \frac{2\pi}{Z\lambda_{\mathrm{eq}}}. \tag{16}$$

To find the torque, we first evaluate the average energy per cell in the ring for several $Z \gg 1$ and both positive and negative curvature, parametrizing it by the radius of curvature c. The torque is then obtained by numerically differentiating the energy [eqn (14)].

The results for small $\beta = 0.6$ and large $\beta = 2.6$ basal tension are shown in Fig. 8. Like in Fig. 6 we combine analytical results for flat epithelia with numerical results for corrugated epithelia. At small apical tension where the stable state is flat, the torque increases as predicted by eqn (15). At the transition to the expanded corrugated epithelium the torque does not seem to change at all and the numerical results follow eqn (15), which is somewhat surprising. We are led to conjecture that this trend

continues in the corrugated state until the transition to the thick flat state.

Bending modulus of epithelial rings

Among the other quantities of interest is the bending modulus. Within the scope of this work, the bending modulus is strictly speaking relevant only for vanishing differential tension where the spontaneous curvature of the cells vanishes. At any nonzero $\alpha - \beta$, the bending modulus really refers to the elasticity of finite ring-like structures rather than to sheet-like uncurved epithelia. This issue is possibly related to the mechanics of small curved structures such as epithelial ducts.[17]

For small $\alpha - \beta$ where the shape of isolated cells is only slightly trapezoidal, cell height and median are approximately the same as in rectangular cells and read $l_l \approx l_{rect} = \sqrt{\alpha + \beta}$ and $l_m = (l_a + l_b)/2 \approx 1/\sqrt{\alpha + \beta}$, respectively. In this case the spontaneous curvature of the tissue c_0 is small and to the lowest order

$$c_0 \approx -2\sqrt{\alpha + \beta}(\alpha - \beta). \quad (17)$$

This result can be recast as $c_0 \approx -2l_l(\alpha - \beta)$ so as to emphasize that the spontaneous curvature is proportional to both differential tension and the distance between the apical and the basal sides l_l. However, this result is not valid for very large β where trapezoids are replaced by triangles. In this case (which also implies tall cells) the spontaneous curvature decreases with β and tends to 0 as $\beta \to \infty$. [We note in passing that the torque of the flat epithelium given by eqn (15) is directly proportional to cell spontaneous curvature.]

The radius of the reference stress-free epithelial rings is equal to $1/c_0$ and they contain $\pi/(\alpha - \beta)$ cells. To compute its bending modulus, we need to consider the energy per unit contour length of the epithelium w_{trap}/l_m. For slightly deformed trapezoidal cells, w_{trap}/l_m is a parabolic function of the curvature

$$\frac{w_{trap}(c)}{l_m} = \frac{w_{trap}(c_0)}{l_m} + \frac{Y}{2}(c - c_0)^2, \quad (18)$$

where Y is the bending modulus. If $\alpha - \beta \ll 1$, the bending modulus can be calculated analytically:

$$Y \approx \frac{1}{4} - \frac{7}{16}(\alpha - \beta)^2. \quad (19)$$

Thus the bending modulus only depends on the differential tension but not on the tissue lateral tension $\alpha + \beta$. As the tissue lateral tension is directly related to tissue thickness $l_l \approx l_{rect} = \sqrt{\alpha + \beta}$, we conclude that at a given differential tension the resistance of a stress-free epithelial rings to bending is the same irrespective of the ratio of tissue thickness and curvature radius. In other words, thick-walled rings with a small lumen are just as deformable as thin-walled rings with a large lumen. The 2D bending would correspond to a lengthwise-uniform deformation of the cross-section of an epithelial tube of radius $1/c_0$ due to, *e.g.*, compression of the tube by two parallel plates.

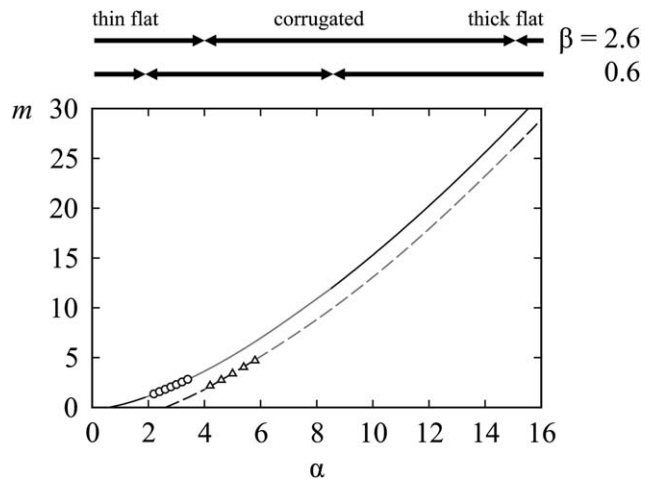

Fig. 8 Average torque per cell *vs.* apical tension at $\beta = 0.6$ and $\beta = 2.6$ (solid and dashed lines, respectively). The torque generally increases with the apical tension (more precisely, with the differential tension $\alpha - \beta$) and not by the transitions between the flat and the corrugated states indicated by the sequences of arrows above the diagram. Symbols represent the numerically computed torque in the corrugated states and gray lines are the continuation of the flat-state torque [eqn (15)] in the regime of the collapsed corrugated state.

Conclusions

Our study of a model simple epithelium shows that internal stresses within the tissue can generate corrugated morphologies of varying wavelengths and roughness. Within the theoretical framework used here, these stresses are induced by the differential apical-basal tension. The main factors involved in the formation of the corrugated epithelia are apical constriction and cell–cell repulsion. Although the model also predicts long-wavelength morphologies, its most robust nontrivial feature is the collapsed corrugated state characterized by a wavelength of the order of cell size. In the regime of intermediate apical and basal tensions where the cells are approximately isometric, the stretching modulus of the corrugated epithelium is much smaller than that of the flat epithelium.

These findings can be related to the morphologies of real epithelial tissues but the comparison is necessarily qualitative because of the reduced dimensionality of our model. In addition, most epithelia are attached to a certain support structure such as the basement membrane or the connective tissue, and the mechanics of the supportive tissue does affect the morphology of the tissue in some way. Comparison is most straightforward in embryonic tissues where the support structures do not play as prominent a role as in the later stages of development, even more so before the deposition of the extracellular matrix when tissues are liquid-like and characterized by an effective surface tension.[19] Certain elements of the phenomenology of the model epithelia discussed here were already mentioned in a related study of ours[15] where localized apical and basal constriction of certain cells in the *Drosophila* ventral furrow were identified as possible factors contributing to the furrow formation. Similarly, localized constriction could participate in the later stages of *Drosophila* morphogenesis, *e.g.*,

in the formation of dorsal folds. The various shape transformations could be explored within a geometrically accurate 3D model of the embryo based on the epithelial mechanics discussed here and in ref. 15, and it will be very interesting to see which features of the *Drosophila* morphogenesis can be reproduced by a simple, single-cell type model.

Despite the above reservations, we must mention two examples of wrinkled epithelial morphologies reminiscent of our model tissues. With their regular periodicity as well as narrow tops and wide bases, the longitudinal folds of the stomach of *Styela clava*,[20,21] an ascidian tunicate, are very similar to our expanded corrugated state (Fig. 2 in ref. 22). From the structural perspective, this epithelium is considerably more complex than our model because it is attached to the connective tissue and because each fold consists of two cell populations (one of them rapidly dividing) rather than a single undividing cell type like in our model. Yet the final contour is very close to those shown in Fig. 3. A related example of an ascidian stomach epithelium is that of *Ciona intestinalis* (sea squirt).[21] Just like in *Styela clava*, the epithelial folds are longitudinal and very regular but the waveform contains a minor and a major fold (Fig. 2E in ref. 21). The details of this morphology are beyond the spectrum of epithelial shapes predicted within our model.

The main features of the longitudinal-fold morphology can also be reproduced within other biomechanical models, *e.g.*, in a sophisticated theory of growing epithelium confined to a rigid tube where the tissue is treated as an anisotropic elastic solid to account for the cross-ply collagen fiber reinforcement.[23] Depending on the anisotropy of the growth rates, this theory also accounts for the lengthwise segmentation of the tissue characteristic of small intestine. Key to these elastic instabilities is spatial confinement rather than internal stresses like in our model. As a result, the folds predicted by the theory of ref. 23 are generally smooth and spread-out so as to minimize the elastic energy rather than hairpin-like as those seen in Fig. 3.

This comparison suggests that by examining the shape of the folds, one may be able to distinguish between the possible scenarios of their formation. Further support for this hypothesis is provided by a theory of epithelial instabilities that reproduces the long-wavelength buckling by invoking the elasticity of the supporting connective tissue.[16] Like in ref. 23, dividing cells within the epithelium exert stresses on the surrounding structures, and the pressure generated by division drives the lateral expansion of epithelium leading to buckling and folding. The final shape of the tissue is corrugated but neither the tips nor the grooves of the folds are very pronounced—in stark contrast with the cusps in our corrugated epithelia driven by differential tension.

Most likely the three mechanisms discussed above (interaction with either rigid or elastic substrate, division-related intra-epithelial pressure, and shear stress caused by differential tension) are active simultaneously, each contributing to the final shape of the tissue. It is possible that the length scales associated with the different mechanisms are separated. Interaction with the substrate could account for the large features of epithelia whereas the internal shear stresses and the cell–cell repulsion could shape the fine morphological details such as the tip of the villus in the intestinal epithelium where the radius of curvature is of the order of cell size and the immediate substrate is barely existent. This hypothesis could be tested by generalizing our model by a thin flexible substrate representing the basement membrane which will make the sharp, hairpin-like folds more round. By increasing the bending modulus of the membrane, we may expect to find a regime where the corrugated epithelium does not feature in the phase diagram. Above all, this extended model would facilitate a direct comparison with experiments simply because of the more realistic geometry.

Also interesting will be the 3D version of the model where the epithelial structures formed by apical or basal constriction should be more diverse than in 2D, including corrugated plane-wave morphologies and various lattices of protrusions and recesses reminiscent of villi and crypts in the intestinal epithelia.[16] All of these morphologies are promoted by the differential apical-basal tension which forces parts of the epithelium into shapes of local non-zero mean curvature just like it produces the hairpin bends seen in the corrugated states in Fig. 3. But in 3D the differential tension will play a far more prominent role than in 2D. For example, in a villus-like protrusion both the tip and the stem have a mean curvature of opposite sign than that of the saddle-shaped base. As a result, the difference between the inner and the outer surface areas can be increased arbitrarily by making the villus longer and longer, thereby lowering the energy until all epithelium area is exhausted. Thus we can expect that the 3D model will produce long and narrow protrusions (if the basal tension is larger than the apical tension) or recesses (if the apical tension exceeds the basal tension).

With the 3D model, we will be able to put its underlying principles to a quantitative test, *e.g.*, by comparing the exact shape of the protrusions or recesses and the number of cells seen in the cross-section. Within the current reduced-dimensionality model, such a comparison is difficult despite qualitative similarity because the fraction of cells in a waveform that undergo apical constriction is inherently smaller than in the 3D model for geometrical reasons mentioned above. In particular, in the corrugated epithelial shapes seen in Fig. 3 only cells in the favorable bend are characterized by the energetically favorable apical constriction whereas in the intestinal crypts as their 3D counterparts all cells along the vertical tube-like portion of the epithelium will undergo apical constriction, albeit not as much as the bottommost cells. In turn, this implies that the number of cells seen in the cross-section of a typical crypt (or a villus) will be considerably larger than N_{eq} in our reduced-dimensionality model corrugated epithelia, quite possibly about 100 like in real intestinal epithelia rather than between 15 and 40 as in the present study (Fig. 4).

The framework discussed here could be extended in several other directions. One possibility is to consider epithelia of cells with non-uniform differential apical-basal tension. This idea relies on the mechanism of self-renewal of intestinal epithelium which includes cell division in the crypts and the migration of the new cells up the sides of the villi towards the tips.[20,24,25] It seems possible that the differential tension of these cells

changes sign as they move from crypts to villi. One could think of either symmetric and asymmetric profiles of the differential tension, each of them affecting the epithelial morphology in a different way. Yet another set of questions includes the stability and the mechanics of the finite-size epithelial structures such as blastulae or kidney ducts. A more ambitious generalization of the model would address the very stability of the simple epithelium, choosing between the single-cell-thick and the stratified or even bulk tissues so as to describe the complex epithelial processes such as intercalation, involution, ingression, and delamination.

Acknowledgements

It is our pleasure to acknowledge numerous discussions with J. Derganc, T. H. Ermak, D. Petrovič, G. Salbreux, and S. Svetina. We are indebted to D. Petrovič for providing the micrograph shown in Fig. 1a. This work was supported by Slovenian Research Agency through Grant no. P1-0055, by Marie Curie Initial Training Network COMPLOIDS Grant FP7-PEOPLE-ITN-2008 no. 234810, and by the ESF Research Networking Programme QuanTissue. A. H. B. is supported by Raymond and Beverly Sackler Fellowship.

References

1 E. Cerda, K. Ravi-Chandar and L. Mahadevan, *Nature*, 2002, **419**, 579–580.
2 E. Sharon, B. Roman, M. Marder, G.-S. Shin and H. L. Swinney, *Nature*, 2002, **419**, 579.
3 Y. Klein, E. Efrati and E. Sharon, *Science*, 2007, **315**, 1116–1120.
4 J. Kim, J. A. Hanna, M. Byun, C. D. Santangelo and R. C. Hayward, *Science*, 2012, **335**, 1201–1205.
5 H. Liang and L. Mahadevan, *Proc. Natl. Acad. Sci. U. S. A.*, 2009, **106**, 22049–22054.
6 R. Keller, A. Davidson and R. Shook, *Differentiation*, 2003, **71**, 171–205.
7 T. Lecuit and P.-F. Lenne, *Nat. Rev. Mol. Cell Biol.*, 2007, **8**, 633–644.
8 A. C. Martin, M. Gelbart, R. Fernandez-Gonzalez, M. Kaschube and E. F. Wieschaus, *J. Cell Biol.*, 2010, **188**, 735–749.
9 G. M. Odell, G. Oster, P. Alberch and B. Burnside, *Dev. Biol.*, 1981, **85**, 446–462.
10 G. W. Brodland, V. Conte, P. G. Cranston, J. Veldhuis, S. Narasimhan, M. S. Hutson, A. Jacinto, F. Ulrich, B. Baum and M. Miodownik, *Proc. Natl. Acad. Sci. U. S. A.*, 2010, **107**, 22111–22116.
11 K. K. Chiou, L. Hufnagel and B. I. Shraiman, *PLoS Comput. Biol.*, 2012, **8**, e1002512.
12 O. Luu, R. David, H. Ninomiya and R. Winklbauer, *Proc. Natl. Acad. Sci. U. S. A.*, 2010, **108**, 4000–4005.
13 M. Leptin and B. Grunewald, *Development*, 1990, **110**, 73–84.
14 J. Derganc, S. Svetina and B. Žekš, *J. Theor. Biol.*, 2009, **260**, 333–339.
15 A. Hočevar Brezavšček, M. Rauzi, M. Leptin and P. Ziherl, *Biophys. J.*, 2012, **103**, 1069–1077.
16 E. Hannezo, J. Prost and J.-F. Joanny, *Phys. Rev. Lett.*, 2011, **107**, 078104.
17 E. Hannezo, J. Prost and J.-F. Joanny, *Phys. Rev. Lett.*, 2012, **109**, 018101.
18 K. Brakke, *Exp. Math.*, 1992, **1**, 145–165; Surface Evolver is available at http://www.susqu.edu/facstaff/b/brakke/evolver/evolver.html.
19 T. Mammoto and D. E. Ingber, *Development*, 2010, **137**, 1407–1420.
20 T. H. Ermak, *J. Exp. Zool.*, 1975, **194**, 449–466.
21 T. H. Ermak, *J. Exp. Zool.*, 1981, **217**, 325–339.
22 T. H. Ermak, *Am. Zool.*, 1982, **22**, 795–805.
23 P. Ciarletta and M. Ben Amar, *J. Mech. Phys. Solids*, 2012, **60**, 525–537.
24 M. Mathan, P. C. Moxey and J. S. Trier, *Am. J. Anat.*, 1975, **146**, 73–92.
25 M. L. Hermiston and J. I. Gordon, *J. Cell Biol.*, 1995, **129**, 489–506.